Int J Adv Manuf Technol (2017) 91:1255–1273
DOI 10.1007/s00170-016-9844-1

ORIGINAL ARTICLE

Experimental validation and characterization of a real-time metrology system for photopolymerization-based stereolithographic additive manufacturing process

Xiayun Zhao[1] · **David W. Rosen**[1]

Received: 12 September 2016 / Accepted: 25 November 2016 / Published online: 3 December 2016

Abstract Exposure Controlled Projection Lithography (ECPL) is a stereolithography-based additive manufacturing process, curing photopolymer parts on a stationary substrate. To improve the process accuracy with a closed-loop control, an in situ interferometric curing monitoring and measurement (ICM&M) system was developed to infer the output of cured height. The authors have previously reported an ICM&M method which consists of a sensor model for the ICM&M system and online parameter estimation algorithms based on instantaneous frequency. In this paper, to validate the ICM&M method, an application program was created in MATLAB to integrate the ECPL and ICM&M systems and to acquire and analyze interferograms online. Given the limited computing power, the ECPL process interferograms were acquired real time and analyzed off-line. A series of experiments was performed curing square samples by varying exposure time and intensity. Results show that the ICM&M can provide a cost-effective measurement for cured heights with excellent accuracy and reliability, and possess decent capability of estimating lateral dimensions. The off-line ICM&M is a convincing demonstration and benchmark for the real-time ICM&M metrology, providing a comprehensive evaluation of the ICM&M system's measurement characteristics as well as its utilities in modeling and control of the additive manufacturing process dynamics.

Keywords Additive manufacturing · Stereolithography · Real-time measurement · Interferometry · Experimental validation · Measurement characteristics · Process dynamics and control · Photopolymer · Refractive index

✉ David W. Rosen
david.rosen@me.gatech.edu

[1] George W. Woodruff School of Mechanical Engineering, Georgia Institute of Technology, Atlanta, GA 30332, USA

1 Introduction

Lack of in situ sensors and measurement methods for in situ process control is identified as high-priority research and development activities for overcoming the barriers in improving the quality and repeatability of additive manufacturing (AM) processes [1]. Improved sensors and controls used in AM equipment and processes can enhance monitoring and control capabilities to provide real-time visibility and control of the building part. Real-time inspection and material property determination during the manufacturing process can improve production of qualified parts directly from the AM machine [2]. Process monitors and controls should be fully integrated with the AM process [3].

In this study, the AM process is a mask-projection stereolithography-based additive manufacturing process denoted as Exposure Controlled Projection Lithography (ECPL), which can cure photopolymer materials into 3D parts on a stationary transparent substrate [4]. To improve the ECPL process accuracy, an in situ metrology is designed to enable an advanced closed-loop control [5]. An interferometric curing monitoring (ICM) system has been developed to visualize the curing process and infer roughly the output of cured height by an implicit model and approximate phase counting which is not fast and accurate enough to measure in-process [6–8]. The authors have previously reported a new interferometric curing monitoring and measurement (ICM&M) method distinguished by a sensor model based on instantaneous frequency and an online parameter estimation algorithm with moving horizon exponentially weighted Fourier curve fitting [9].

The paper details the authors' initial efforts to validate the ICM&M model and algorithms, as described in [9]. In particular, the comparison of ICM&M and microscope-measured cured part dimensions, primarily vertical height, is presented. "Section 2" introduces the physical system and "Section 3" introduces the experimental methodology including the real-time measurement method. "Section 4" shows the experimental validation results and "Section 5" discusses the measurement characteristics and utilities of the ICM&M system. Given the limited equipment configurations, an off-line analysis is performed, instead of real-time ICM&M, by analyzing the real-time acquired interferogram video and simultaneously estimating the cured height. Please note that the real-time ICM&M and off-line ICM&M share exactly the same sensor model and algorithms, and the only reason we cannot achieve complete real-time ICM&M is because it demands much more computation power.

2 System overview

The overall physical system of the in-house-designed additive manufacturing machine, as illustrated in Fig. 1, consists of two core modules: the ECPL system (shown in the bottom blue frame) and ICM&M system (shown in the top green frame). Details about the systems have been reported in literature [4].

The ECPL system aims to deliver a serial of timed and patterned ultraviolet (UV) light beams into the resin chamber where photopolymerization occurs to form a 3D object. The UV light, homogenized by the beam conditioning system and shaped by digital micromirror device (DMD), is projected through the bottom transparent substrate of the resin chamber into the photopolymer resin.

The ICM&M system is based on a Mach-Zehnder interferometer [8]. A coherent laser shines through a beam expander, moveable iris, and beam splitter, onto the resin chamber. Light reflecting off the interface surfaces of the resin chamber reflects through the beam splitter and into the camera. Due to the optical path differences between the light beams reflected from different interface surfaces, an interference pattern is observed by the camera.

3 Experimental methodology

3.1 ICM&M method

To improve the process accuracy with closed-loop control for ECPL, an interferometric curing monitoring and measuring method was developed, addressing the sensor modeling and algorithm issues [9, 10]. In the previously reported literature, a physical sensor model for ICM&M was derived based on interference optics utilizing the concept of instantaneous

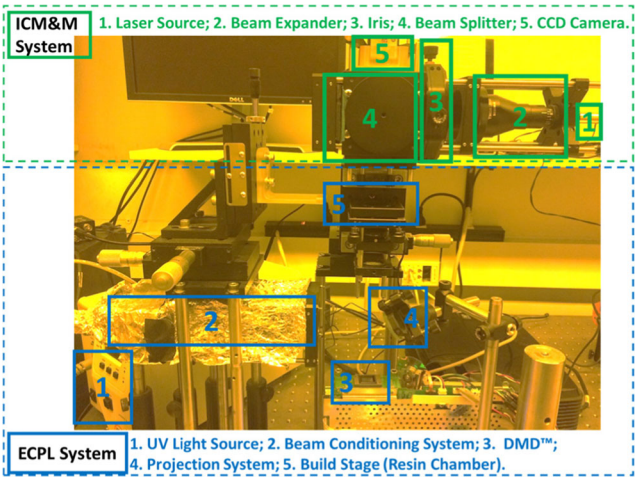

Fig. 1 Overall physical system: the ECPL system integrated with the ICM&M system

frequency. The associated calibration procedure was outlined for ICM&M measurement accuracy [10]. To solve the sensor model, particularly in real time, an online evolutionary parameter estimation algorithm was developed adopting moving horizon exponentially weighted Fourier curve fitting and numerical integration [9, 10].

Figure 2 presents a summary of the ICM&M method illustrating the relationships among the charge-coupled device (CCD) camera, the acquired interferogram data, the sensor model, and online algorithms. The ICM&M sensor model is developed to sense the local derivative in the interference pattern and provides a formulated problem for the parameter estimation and cured height algorithms to solve. The implicit model interprets the observed interferogram intensity (I_M) in terms of the cured height (Z), refractive indices (n_m, n_l), amplitudes (I_0, I_1), and phase offset φ, all of which are unknown and dynamically changing; hence, the cured height Z is unsolvable by a single observation of intensity at one time point. The time derivative of Z corresponds to the curing velocity denoted as $\dot{Z}$. A time sequence of the intensity signal is needed to depict a sequence of instantaneous frequency resulting from the curing velocity, and thereby the total phase angle $\sum_i T_i f_i$ can be evaluated resulting in the cured height Z as shown in the explicit sensor model.

The algorithm of parameter estimation by moving horizon exponentially weighted "fourier1" curve fitting is developed to estimate the instantaneous frequency f in the sensor model. Note that all the blue symbols in Fig. 2 denote frequency items and mappings between the model and algorithms. This procedure needs to be repeated for each subsequent time period as the part is being fabricated. When part fabrication is completed, an estimate of the total interferogram phase angle and total cured part height is produced.

To implement the measurement of cured height during the online operation with the ECPL system, an ICM&M calibration procedure should be performed beforehand to estimate

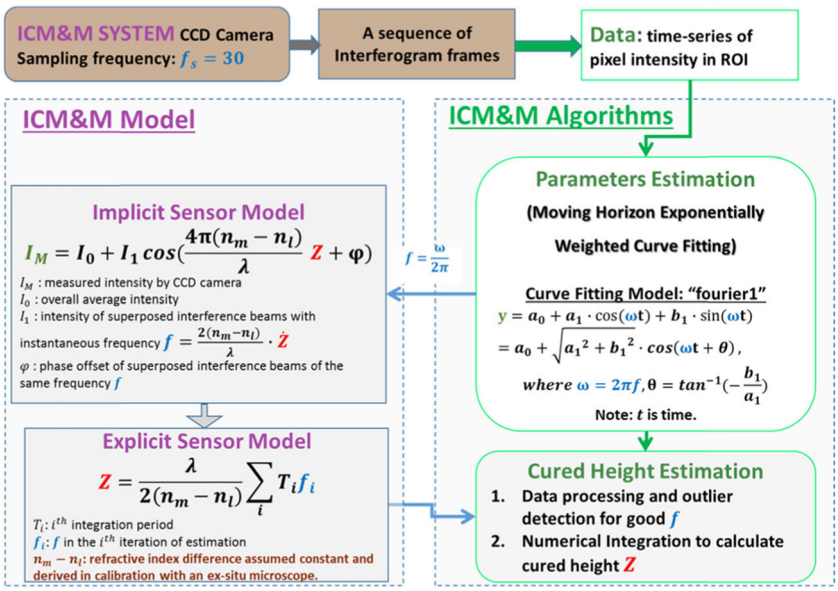

Fig. 2 Scheme of ICM&M sensor method: models and algorithms [10]

the key index of refraction differences between the solid and liquid resins off-line. The overall scheme of the developed ICM&M method with evolutionary estimation and incremental accumulation enables a promising real-time implementation which will be investigated experimentally in this paper.

3.2 MATLAB application for implementing the ICM&M method

As the ICM&M method is developed specifically for the ECPL process, to validate the method, a software is desired for implementing the ICM&M method along with the ECPL system. A MATLAB application was created to serve as a testing platform in this study as well as a prototype software for a future synthesized ECPL machine.

3.2.1 Software tasks

A graphical user interface using the graphical user interface development environment (GUIDE) of MATLAB was created to implement the ICM&M method for the ECPL process. The application was designed to streamline the operation of the ECPL process with the ICM&M acquisition and measurement analysis. The software interfaces with the hardware of the ECPL system's ultraviolet lamp and DMD and the ICM&M system's camera. It logs the acquired interferogram video data, performs numerical computations with the ICM&M algorithms, and saves the measurement results for all voxels in the region of interest.

3.2.2 Computation environment

The application is executable in MATLAB R2015b for a 64-bit operating system and can be used in both experiment and post analysis. The real-time acquisition of the ECPL process was done in situ on the lab desktop computer with a processor of Intel® Core(7M) i7 CPU 870 @2.93GHz 2.94GHz and an installed memory (RAM) of 16.0 GB (8.00 GB usable). All the off-line ICM&M analysis was done on an ex situ Lenovo laptop with Intel(R) Core(TM) i7-4510U CPU @ 2.00GHz 2.6 GHz and an installed memory (RAM) of 8.00 GB. Provided a more powerful multicore processor and a high-speed camera, the ICM&M is expected to be able to run faster and perform more accurate measurement online with a full-field measurement capability if necessary.

3.3 Experiment design

According to the ICM&M sensor model and calibration process [10], the experiment design incorporates a calibration experiment and a set of validation experiments.

3.3.1 Design philosophy and experiment plan

As presented in the previous paper [10], a calibration procedure is required to determine the uncertain material property of the refractive index in the ICM&M method. The design of the ICM&M method possesses measurement traceability by relating its measurements to a known standard. In this study, the Olympus LEXT OLS4000 3D material confocal microscope [11] is used to measure sample height profile. For each new batch of material, calibration is performed once at the beginning and more times later if necessary. The derived refractive index value from calibration is assumed to be constant under the normal ECPL operating conditions so that the ICM&M measurement results are within engineering tolerance over some reasonable period of time. In this study, a

bottle of material resin was prepared and used in all the experiments which were done over a period of about 2 weeks.

To validate the feasibility and explore the capability of the developed ICM&M method, two series of validation experiments were designed to cure 3D square blocks for various exposure time and under different UV intensities, respectively. Each experiment category above has its own particular purpose; meanwhile, together they serve to provide a thorough investigation with one common theme—to demonstrate that the ICM&M method is reproducible and robust in measuring cured parts with precision and accuracy. Table 1 presents the overall scheme of the designed experiment that consists of one calibration experiment and two validation groups. The varying process conditions for each validation group are italicized.

For each individual experiment that cures a square block within certain conditions (i.e., DMD bitmap size, UV intensity, and exposure time), the curing process was captured by the ICM&M camera in real time with an acquisition speed of 30 frames/s and saved into a video file along with the process data including the UV lamp close time. Thereafter, in the "Offline Measurement" module in the MATLAB application, the video of interferograms and all process data were loaded ex situ at a laptop computer and analyzed to obtain the cured height profile for a selected region of interest (ROI). The cured part was also measured by the confocal microscope, of which the measurement result was used as the actual height to compare with the off-line ICM&M measurement result for error analysis.

3.3.2 ICM&M implementation

In the implementation and investigation of the ICM&M method, there are a few practical thoughts to address in the experiment design.

First of all, choosing square blocks as target 3D objects in the experiments is because the resultant cured part with lateral aspect ratio close to if not equal to 1:1 from the square bitmap projection could vividly demonstrate that the ECPL process is isotropic and homogeneous, and that the ICM&M method is omnidirectional. Besides, square blocks provide a simple and efficient way of testing the accuracy of ICM&M by presenting obviously flat height profiles. In principle, one can always use various DMD bitmaps to cure customized parts and utilize the same ICM&M method which should be universally applicable for measuring cured height profile regardless of the part shape.

Ideally, measuring a height profile with ICM&M means measuring the cured heights of all voxels based on all the pixels in the ROI, which would be computationally tedious and costly especially in real-time ICM&M. The cured part is supposed to have a uniform height profile due to ideally uniform UV light intensity and material properties across the curing area; hence, the adjacent pixels are supposed to have very similar if not identical changed phase angles during the curing process. Pixels' time sequences of grayscale in interferograms were compared, confirming the assumption of the proximity similarity in neighboring pixels' profile. It has been found that to evaluate the height profile, measuring heights for pixels in the ROI at an interval of 5 pixels would not affect the accuracy significantly but requires much less computation expense than measuring every pixel for the whole area. Specifically, we measured every 5 pixels because (1) a 5-by-5 image median filter was used to denoise the raw data, hence measuring every 5 pixels does not omit or overlap any raw data; (2) it turns out that measuring every 1 pixel does not improve the accuracy significantly but requires far more computations. According to the recommended practice, the pixels in the measured area's line profile is denoted in the form of Pixels (starting pixel width coordinate: interval: ending pixel width coordinate, starting pixel height coordinate: interval: ending pixel height coordinate). For example, Pixels (245:5:365, 220) denotes a horizontal line of

Table 1 Experimental design matrix

		Experiment groups		
		Calibration	Validation group #1: varying exposure time	Validation group #1: varying exposure intensity
Experiment setting	Exposure time (s)	12	*9, 12, 15*	12
	Exposure intensity (UV iris level)	22%	22%	*40%, 35%, 30%, 25%, 20%, 15%, 10%, 5%*
	Exposure pattern bitmap size (pixels × pixels)	250 × 250	250 × 250	250 × 250
Particular attributes to assess for the ICM&M method		Traceability	Temporal stability	Sensitivity
Common attributes to assess for the ICM&M method		1. External and internal comparability 2. Precision and accuracy 3. Resolution and range 4. Repeatability		

25 pixels starting from Pixel (245, 220) to Pixel (365, 220) with 5 pixels between each two neighboring measured pixels.

Since the nonuniform acquisition is averagely 30 frames/s, this study performed a measurement every ten frames of interferogram, correspondingly at a temporal measurement period of approximately 1/3 s.

Lastly, because the UV lamp in the ECPL system is designed for users to adjust its intensity in percentage scale of the "iris level"; for example, 100% means a fully open iris and maximum intensity and 0% means completely closed and no irradiation at all. Hence, we used the iris level as a nominal indication of the exposure intensity applied in the ECPL process.

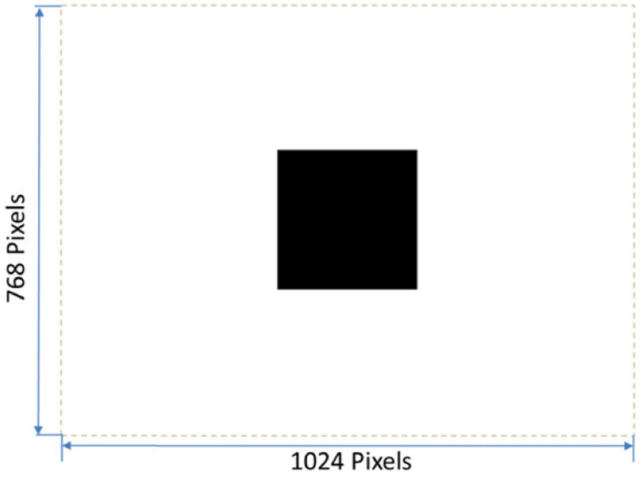

Fig. 3 DMD pattern: 1024 × 768-pixel binary bitmap displaying a black square of 250 × 250 pixels in the center

4 Results and discussion

4.1 Material formulation

As specified in earlier research [4], a trifunctional acrylate monomer—trimethylolpropane triacrylate (TMPTA, SR-351) obtained from Sartomer—was used as obtained, with the photoinitiator 2, 2-dimethoxy-1, 2-diphenylethan-1-one (DMPA, IRGACURE-651) obtained from Ciba Specialty Chemicals, as the resin composition for the ECPL process. The DMPA photoinitiator concentration in the TMPTA monomer was recommended to be 20% by weight to ensure a homogenous solution. This specific formulation required less than 30 s to cure a thick (hundreds of microns) layer of resin. In principle, a resin formulation with a higher sensitivity could have been appropriate for ECPL. However, a fast-curing resin system would impose a higher demand on faster and more accurate measurement and control; hence, the 20% resin formulation mentioned above was used. All the experiments done in this paper used the same bottle of material which consists of a 4:1 ratio by weight of TMPTA monomer (16 g) and DMPA initiator (4 g). The mixture was stirred for approximately 4 h to form a homogeneous solution.

4.2 Calibration experiment

According to the experiment design presented above, for the calibration, a moderate UV intensity corresponding to the UV lamp (OmniCure® S2000) iris level at 22% was chosen so that the ECPL process cured height would not grow too fast or too slow. A 250 × 250-pixel square as shown in Fig. 3 was displayed on DMD for 12 s.

The ICM&M camera captured the video of interferograms when the square block part was cured by the ECPL system. To start the off-line ICM&M analysis, firstly, the interferogram video was replayed in the MATLAB application and the last frame of interferograms which shows the final cured part shape was extracted. In the video's last interferogram as shown in Fig. 4, the ROI was selected by human eye recognition of the cured part outline, approximated by an area of 150 × 150 pixels denoted as Pixels (235:385, 140:290) which is formed by the four corner pixels along with the outline (red dashed line).

The ICM&M method was applied to the square area of 31 × 31 (961) pixels designated as Pixels (235:5:385, 140:5:290), with 5 pixels between each two neighboring measured pixels in both width and height directions. The ICM&M model and algorithm estimated the total phase angle, $\sum_{i}(T_i f_i)$ in Fig. 2, for each measured pixel; and the average total phase angle is 6.150 cycles (i.e., 6.150 × 2π rad) as shown in Fig. 5.

The cured sample was measured by the laser confocal microscope and the average height is 73.492 μm, which substitutes Z in the sensor model equation in Fig. 2. The calibration process is completed by solving the equation:

$\Delta n = n_m - n_l = \frac{\lambda \sum_i (T_i f_i)}{2Z} = 0.022259$, of which the value will be used in the validation experiments to calculate the example part heights to validate the ICM&M measurement capability and accuracy. The corresponding mean solid part refractive index n_m is derived to be 1.49456.

To assess the calibration result, the experiment above was repeated and a second sample was measured with the ICM&M method and the microscope.

The two calibration experiments are summarized in Table 2. The two samples demonstrate great reproducibility of the ECPL process and good consistency in ICM&M. The nuance in the phase angle and microscope measurement lead to a difference at the fourth decimal place of Δn. It is expected that there would be

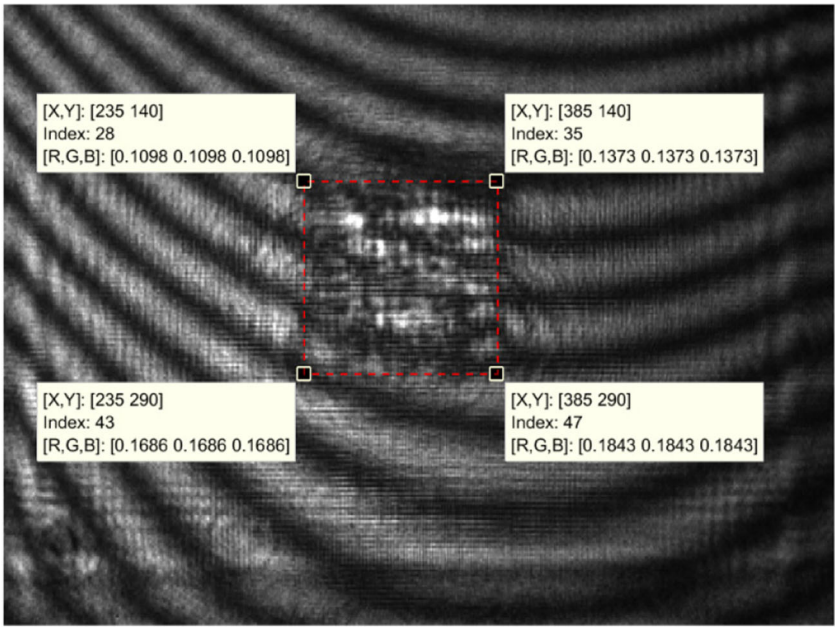

Fig. 4 Calibration: outline of the cured part in the last interferogram—ROI of Pixels (235:5:385, 140:5:290) to be measured

a dispersion of Δn (n_m as well) if one conducts more calibration experiments, because there are always some inevitable process variances and the calibration output of the refractive index is very sensitive to the inputs. Averaging the two calibration results and rounding it to the fourth decimal, we obtained $\Delta n = 0.0222$, correspondingly $n_m = 1.4945$, of which the value will be used in the category of validation experiments to calculate the example part heights to validate the ICM&M measurement capability and accuracy.

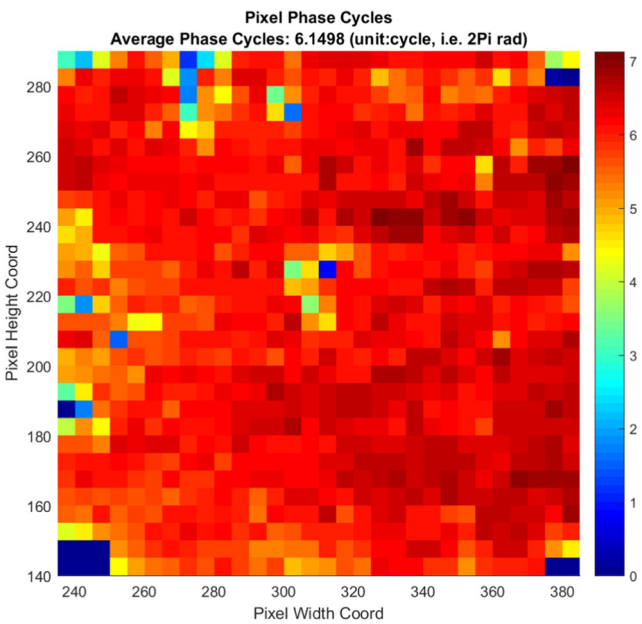

Fig. 5 Calibration: estimated individual and average total phase angles for 31 × 31 pixels in the ROI of Pixels (235:5:385, 140:5:290)

4.3 Validation experiment group #1: varying exposure time

We used the same batch of resin material to further validate the ICM&M model and algorithms reported in a previous paper [10]. In the first set of validation experiments, we cured square blocks by displaying the same size (i.e., 250 × 250 pixels) DMD bitmap under the same UV lamp iris level of 22% as in the calibration process, but for different lengths of exposure time—9 s (Experiment #1), 12 s (Experiment #2), and 15 s (Experiment #3), respectively.

Two samples were cured and measured in each subgroup of exposure time experiments. We will present one sample in each subgroup as an illustration of implementing the ECPL process and ICM&M measurement and later introduce the other sample in each subgroup to demonstrate one important characteristics of process measurement—repeatability in both the ECPL process output and ICM&M measurement result with expected deviations.

The first sample in each subgroup of the experiments with various exposure times was introduced in this section. The off-line ICM&M measurement procedure was illustrated via this set of samples and microscope measurement results were shown to verify the ICM&M results.

Figure 6 displays the ROI for measurement in the experiments and the datatips provide the pixel coordinates (width and height) for the end pixels of the selected line (cyan solid line in the figure) and the corner pixels of the approximated cured shape (red dashed line in the figure). As noted in Fig. 6, the ending interferogram of each experiment shows a clear square shape of about 145 pixels, demonstrating that the ECPL process could preserve the cross-sectional shape and

Table 2 Calibration experiment results

Exp. no.	Number of ROI Pixels	Average of total phase angle estimated by ICM&M (rad)	Average of cured height measured by microscope (μm)	Refractive index difference	Cured part refractive index n_m
1	150 × 150	6.150 × 2π	73.492	0.022259	1.49456
2	145 × 145	6.181 × 2π	74.289	0.022131	1.49443

output a consistent size, in which shape and size both can be well captured by the ICM&M system. As in the calibration process, for each ROI, only these pixels at an interval of every 5 pixels are measured to save computation time at little expense of accuracy. The measured pixels are shown as the selected horizontal lines in Fig. 6.

With the chosen ROI pixels corresponding to the to-be-measured voxels, we simulated the real-time ICM&M method by replaying the video and simultaneously extracting the time series of grayscales for all the measured pixels, followed immediately by estimating the instantaneous frequency and totaling the changed phase angle which leads to the final computing of the cured heights as per the algorithms presented in literature [10]. To illustrate the details of ICM&M algorithm implementation, the sequence of figures in Fig. 7 depicts the time sequence of grayscale intensities, estimated instantaneous frequency along the time, and time curve of cured height for a typical pixel in each experiment, specifically, Pixel (220, 325), Pixel (230, 260), and Pixel (220, 280) in Experiments #1, #2, and #3, respectively.

In Fig. 7a, the grayscale has a range of [0, 255] expressing the intensity of the pixel in the interferograms captured by the CCD camera. It is not exactly sinusoidal due to the nonlinear curing process and stochastic noises including the nonlinear response of camera electronics [12]. The blue dots in the figure depict the signal data and the red line is the fitted curve by the online parameter estimation algorithm. The fitted curve agrees very well with the data, demonstrating the effectiveness of the moving horizon curve fitting and capability of real-time measuring.

In Fig. 7b, we estimated the instantaneous frequency consecutively every ten frames which provided a new batch of ten raw grayscale data points. The measurement period, e.g., ten samples (frames) per run of measurement in this study, could be adjusted based on the computation power; and a sufficiently fast measurement is preferred to capture the process dynamic better so as to measure the process output more accurately.

Figure 7b also shows the cumulative sum of total phase angles during the ECPL process. As the curing process proceeds, the running phase angle change is computed using the expression $\sum_i T_i f_i$ in Fig. 2 to calculate the voxel's cured height as shown in Fig. 7c. The total phase angle is estimated to be 5.206 cycles producing the cured height of 62.38 μm for the voxel on Pixel (220, 325) in Experiment #1. Similarly, in Experiment #2, the total phase angle is 6.060 cycles resulting in an estimated height of 72.61 μm. In Experiment #3, the total phase angle is 7.028 cycles and the estimated height is 84.21 μm. These typical voxel heights estimated by the ICM&M are reasonably close to the microscope measurement as will be depicted in Fig. 8.

In Fig. 7b, another thing worthy to be pointed out is that the estimated instantaneous frequencies in the three experiments are shown to be alike in the first 9 s, which makes sense because the 12- and 15-s exposed curing experiments are actually a temporal extension of the 9-s curing under the same process conditions.

The stereolithographic cure process involves mass and energy transports during the curing process, incorporating exposure and dark reaction [13, 14], as it is vividly shown in Fig. 7a that the pixel grayscale oscillation still persisted for a while

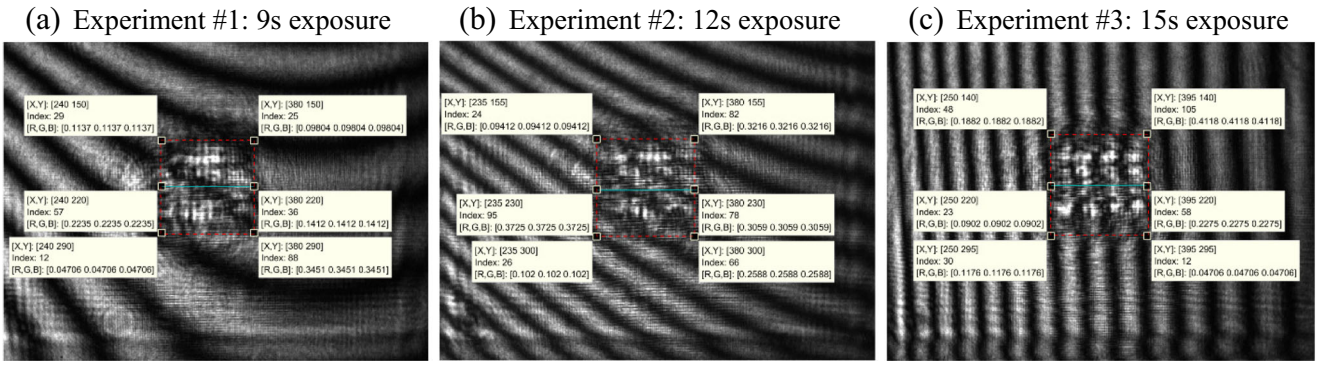

Fig. 6 Selected ROI pixels (*red dashed lines* estimated entire cured area; *cyan line* an example profile line) to measure with ICM&M in the first sample. **a** Experiment #1 9-s exposure. **b** Experiment #2 12-s exposure. **c** Experiment #3 15-s exposure

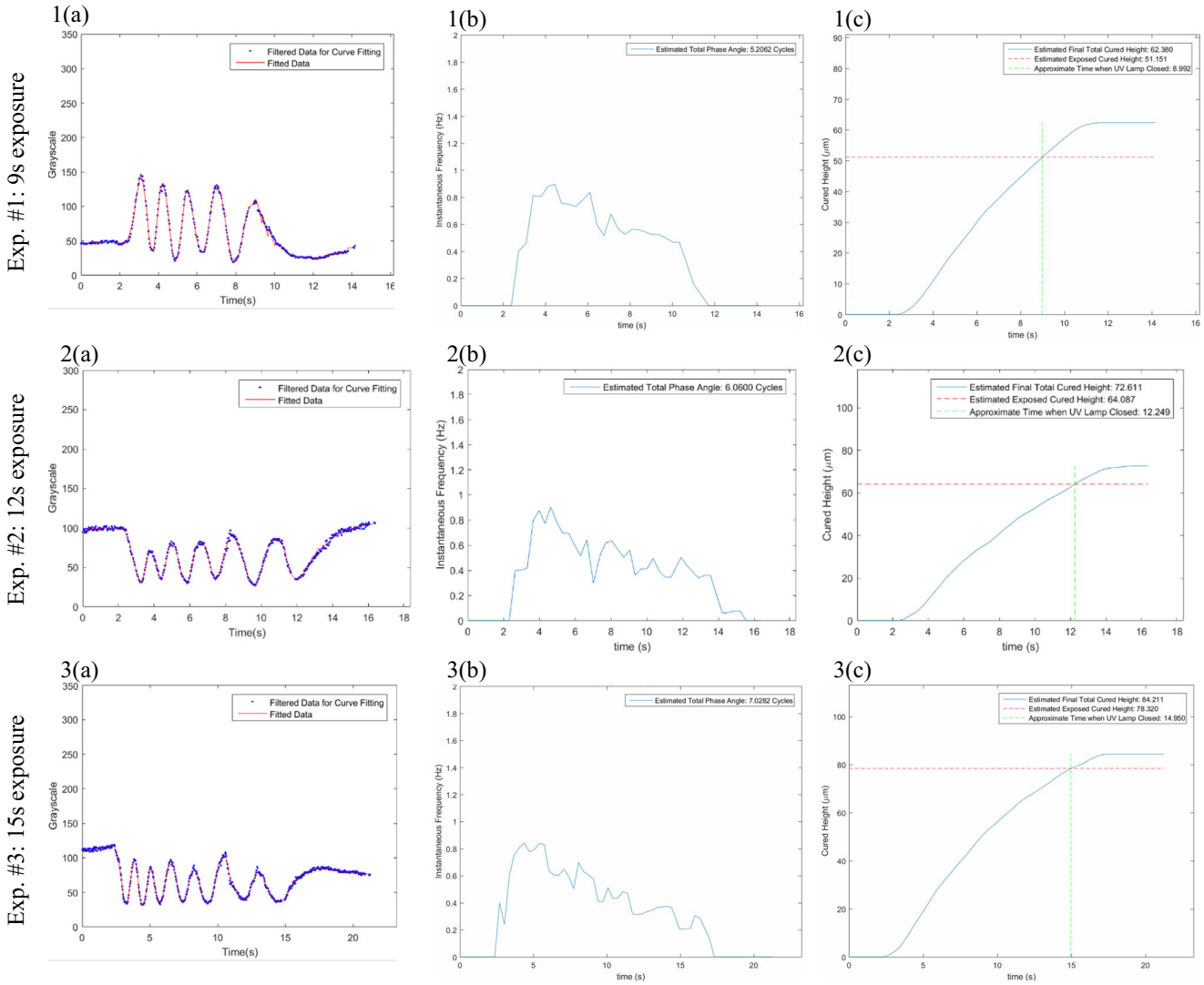

Fig. 7 Illustration of implementing the ICM&M algorithms using the first samples in the experiments varying exposure times. *a* Typical time sequence of grayscale. *b* Estimated instantaneous frequency along the timeline. *c* Evolving cured height of the voxel on the selected pixel

after the UV light was turned off at 9, 12, and 15 s, respectively. As continued "dark" gelation is expected in photopolymerization [15], the cured height by the ECPL process can also be classified into exposed and dark cured heights. Figure 7c marks the UV lamp shutdown time and displays the exposed cured height. The ECPL process is continuous while the ICM&M measurement is discrete with the digital signal measured every ten frames—0.333 s with the camera acquisition speed being 30 frames/s. Hence, there is an error of up to 0.333 s in the approximated UV close time.

As explained in the design of experiments, a single pixel measurement could not be sufficient or conclusive. More pixels need to be measured for final height estimation with less bias. We carried out the same procedure illustrated above to calculate the cured height for all the other voxels on the selected line of pixels (cyan solid line) in Fig. 6 and evaluated the average height as the final result. As a result, the line height profile measured by ICM&M is represented by 30 pixels in all three experiments with an estimated average as detailed in Table 3.

To get a more comprehensive assessment of the ICM&M measurement capability, the entire cured area (enclosed by the red dashed line in Fig. 6, approximatel;y 145 × 145 pixels), was also measured at an interval of 5 pixels, thus the 31 × 31 (961) voxel heights constitute the full-field height measurement as shown in Fig. 8a. The cured area height profile is evaluated with both average and deviation as presented in Fig. 8a.

The cured parts in the experiments were measured with the Olympus 3D confocal microscope as shown in Fig. 8b. The "Height" value displayed at the right-bottom box of the confocal microscope screenshot in Fig. 8b indicates the measured height for the selected profile line. As pointed out in the experiment design, the average of measured heights for two lines

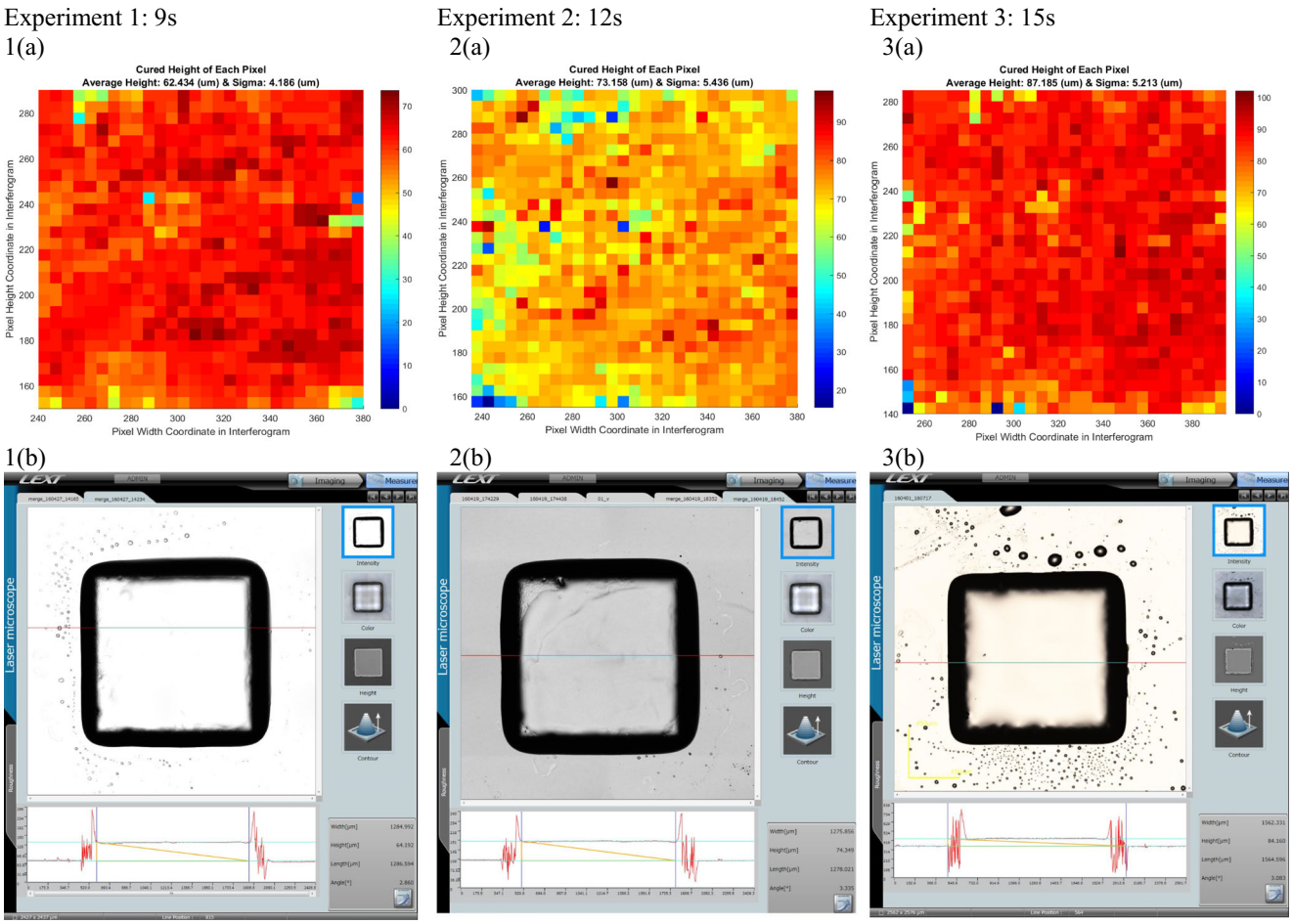

Fig. 8 ICM&M result vs. microscope measurement for the first set of samples in exposure time experiment. Each sample's *a* entire cured area height profile estimated by ICM&M; *b* horizontal profile line in the confocal microscope

Table 3 Measurement results of validation experiments varying exposure time

Experiment Subgroup NO.	Exposure Time (s)	Sample NO.	ROI Pixels (Width, Height)	ICM&M Results			Microscope Measured Profile Line Height (μm)			Absolute Deviation (μm)	Relative Error
				Total Phase (cycle, i.e. 2π rad)	Cured Height (μm)	St.Deviation - Cured Height σ (μm)	X-direction	Y-direction	Average		
Experiment #1	9	Sample 1	Profile Line (240:380, 220)	5.175	62.01	4.19	64.192	63.211	63.70	-1.69	-2.66%
			Cured Area (240:380, 150:290)	5.211	62.43					-1.27	-1.99%
	9	Sample 2	Profile Line (225:370, 220)	5.037	60.35	4.37	63.031	63.335	63.18	-2.83	-4.48%
			Cured Area (225:370, 145:290)	5.144	61.63					-1.55	-2.45%
Experiment #2	12	Sample 1	Profile Line (235:380, 230)	6.065	72.67	5.44	74.349	71.775	73.06	-0.40	-0.54%
			Cured Area (235:380, 155:300)	6.106	73.16					0.10	0.13%
	12	Sample 2	Profile Line (235:380, 200)	6.102	73.11	4.95	72.760	72.299	72.53	0.58	0.80%
			Cured Area (235:380, 135:280)	6.062	72.63					0.10	0.14%
Experiment #3	15	Sample 1	Profile Line (250:395, 220)	7.086	84.91	5.21	84.160	86.329	85.24	-0.34	-0.40%
			Cured Area (250:395, 140:285)	7.276	87.19					1.94	2.28%
	15	Sample 2	Profile Line (225:370, 245)	7.066	84.67	5.45	84.305	83.772	84.04	0.63	0.75%
			Cured Area (230:375, 150:295)	7.129	85.42					1.38	1.64%

in the X-direction (horizontal) and Y-direction (vertical) is used as the final microscope measured height result to reduce the sample measurement bias. The same ECPL process and ICM&M method was repeated once to cure and measure a second square part in each experiment subgroup to investigate the ICM&M system's reproducibility and reliability. Sometimes, the process signals might be too noisy due to the camera hardware heating issue or sometimes the cured part suffered severe defects during washing. All the numerical results will be summarized in Table 3.

In Fig. 8, some tiny holes and uneven surface with bumps and pits are seen in the microscope images of cured samples, which strongly imply that careful handling and postprocessing of the samples is needed. It is worth to point out that the observed sample defects would not affect the height measurement significantly as long as an intact profile line is chosen to measure under the microscope.

As noted in the ICM&M estimated cured height profile in Fig. 8 and Table 3, there is a deviation of around 5 μm in each sample. The deviation was mainly caused by the process and signal noise which led to some deficiency in the ICM&M algorithm. Nevertheless, the average value demonstrates a good accordance with the microscope measurement average and good agreement between the same-condition samples.

Table 3 quantitatively compares the measurement results in terms of absolute error and relative error. For each sample, the two rows in the table represent two different methods of estimating part height. The first row utilizes a method that averages two profile lines, while the second row averages heights across the entire cured area. The brown entries report these cured area height estimates and errors. Results show up to 2-μm absolute deviation and less than 3% relative error. The agreement between the ICM&M estimation result (green column) and the confocal laser microscope measurements (gray column) demonstrates that the ICM&M method is capable of measuring the vertical height for ECPL cured parts with discernment for micron order difference and measurement range of about 100 μm.

Furthermore, in Table 3, comparing the between-sample differences within the same subgroups, we obtained internal consistency for samples cured under the same conditions in ICM&M measurement results despite of the microns' difference, which is also present in the microscope measurement results. The results show that ICM&M is capable of measuring the height of parts cured for likely exposure durations with both accuracy and precision.

As shown in Table 3, Experiment #2 with a 12-s exposure had the smallest errors between ICM&M and microscope, which makes sense because of the identical process conditions as adopted in the calibration experiments. In Experiment #1 and #3 with 9- and 15-s exposures, respectively, the ICM&M was still able to estimate the cured height with great accuracy, despite relatively larger errors. Reasons for the errors will be discussed later in "Section 5.1."

4.4 Validation experiment group #2: varying exposure intensity

In the second set of validation experiments, we cured square blocks by displaying the same size (i.e., 250 × 250 pixels) DMD bitmap for the same length of exposure time (12 s), but under eight different UV intensities corresponding to the UV lamp iris levels at 40, 35, 30, 25, 20, 15, 10, and 5%, respectively. The procedure of ICM&M implementation and microscope measurement was the same as presented in the previous section about the experiments varying exposure times.

For each intensity level, we cured two samples and measured each sample with the off-line ICM&M module in the developed MATLAB application and the confocal microscope. For validation purposes, we compared each individual ICM&M measurement with the microscope measurement result which is the average of two profile line measurement results for each sample.

To demonstrate the ECPL process difference under different intensities and how the ICM&M method responds to the process changes, we presented a representative pixel's interferogram grayscale signal and the ICM&M method's evolutionary estimation of the instantaneous frequency and cured height, as shown in Fig. 9.

In Fig. 9 (left column 1a–8a), the grayscale signals vividly reflect the process dynamics difference due to the UV intensity variations. Conforming to the photopolymerization mechanism, the higher UV light intensity is provided, the more photo initiators are in the process, and the quicker the curing is. Within the same exposure time of 12 s, there was almost one more cycle in 40%-iris-level UV curing than that in the 35%-iris-level curing, which had about a half cycle more than the 30%-iris-level UV curing did, and so on and so forth down to the 5%-iris-level curing.

The process dynamics change caused by the varying intensity is further confirmed in Fig. 9 (center column 1b–8b), which shows that the estimated instantaneous frequencies is larger for the higher-UV-intensity-induced ECPL process. The time curves of cured height measured by the ICM&M are displayed in Fig. 9 (right column 1c–8c) with both exposed and dark cured height values determined when the UV lamp was closed during the ECPL process. Examining into the curing start time in Fig. 9b and c, one could see that the ICM&M estimated time curves of frequency and height have correctly reflected the trend of increasing threshold period in photopolymerization-based AM process with decreasing

exposure intensity [16]. As obviously shown in Fig. 9b and c, the threshold period for 40%-iris UV curing is less than 2 s, while that for 5%-iris UV curing is about 14 s.

Figure 10 depicts three experiments' height profile measurement results for Experiment #3, #4, and #6 with UV iris level being 30, 25, and 15%, respectively. The other subgroups of experiments were performed in a similar way and all the results will be summarized at the end of this section. In Fig. 10a, the selected ROI of approximated cured shape is shown in the ending interferogram of the sample in each experiment. Figure 10b displays the ICM&M estimated heights for the pixels in the ROI at an interval of 5 pixels and similar variations present in the heights profile as seen and explained in the previous validation experiment group. Figure 10c shows the measured profile lines in the X-direction, which demonstrate some variation of a few microns in the profile line; hence, the average of two profile line height values was used as an estimation of the actual cured height to assess the ICM&M results as shown in Table 4.

As a quantitative summary, Table 4 reports in details all the measurement results for the two sets of experiments varying exposure intensities. The experiments with exposure intensity at iris level of 20, 25, 30, and 35% had under 3-μm deviation and less than 5% relative error, while the other experiments at

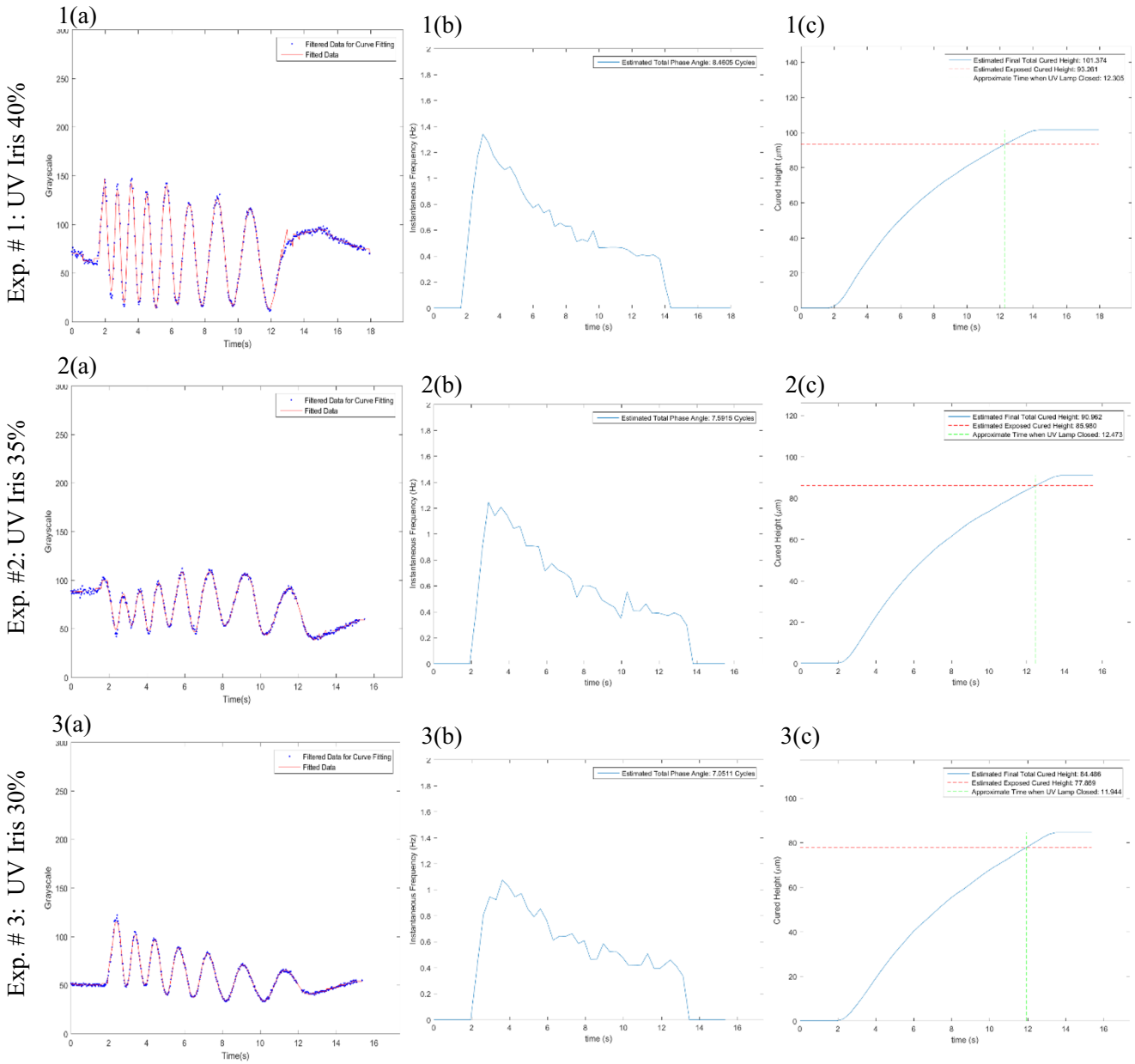

Fig. 9 Process dynamics unfolded by implementing the ICM&M algorithms in the experiments varying exposure intensity: *a* typical time sequence of grayscale; *b* estimated instantaneous frequency along the timeline; *c* evolving cured height of the voxel on the selected pixel

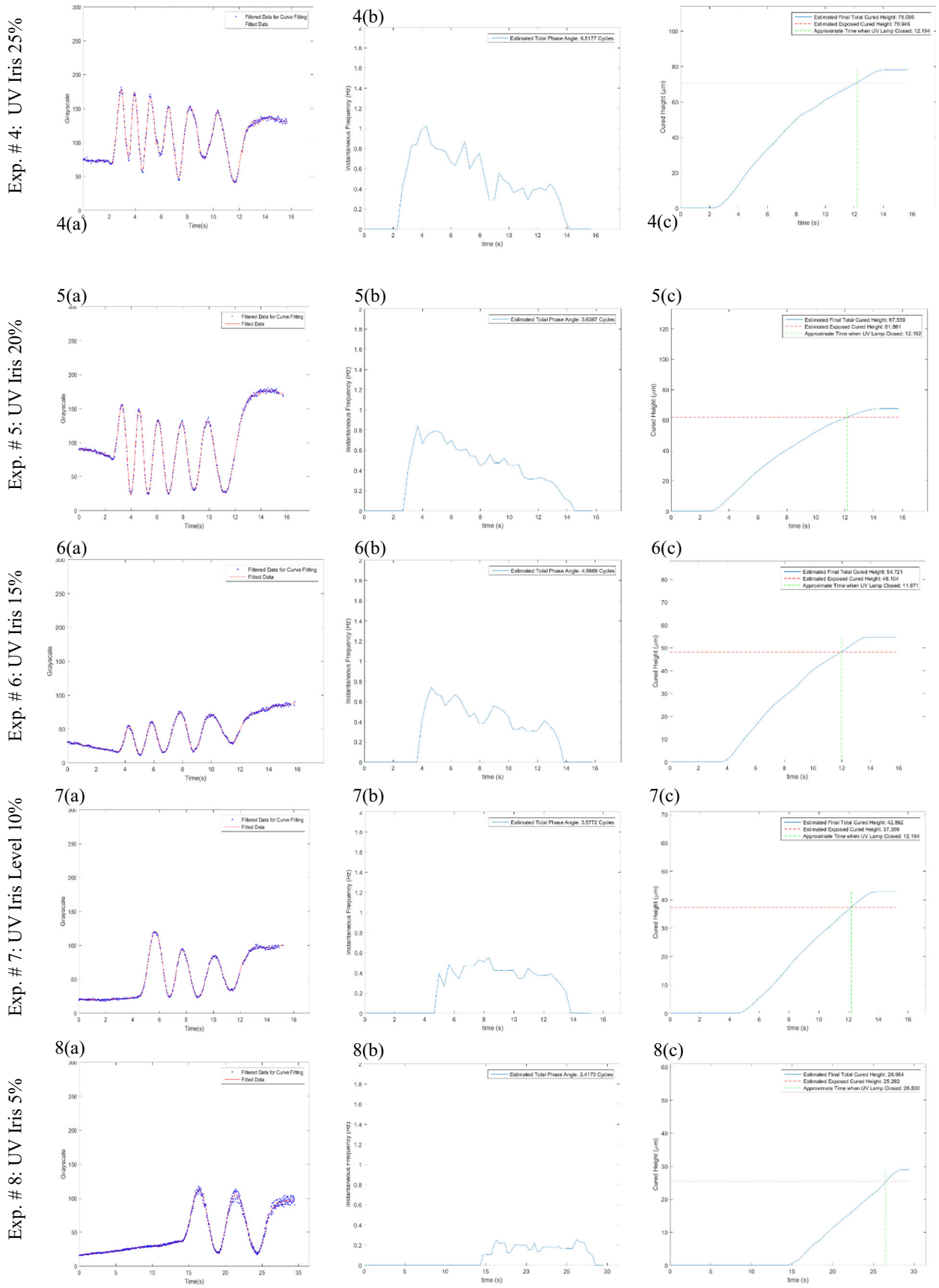

Fig. 9 continued.

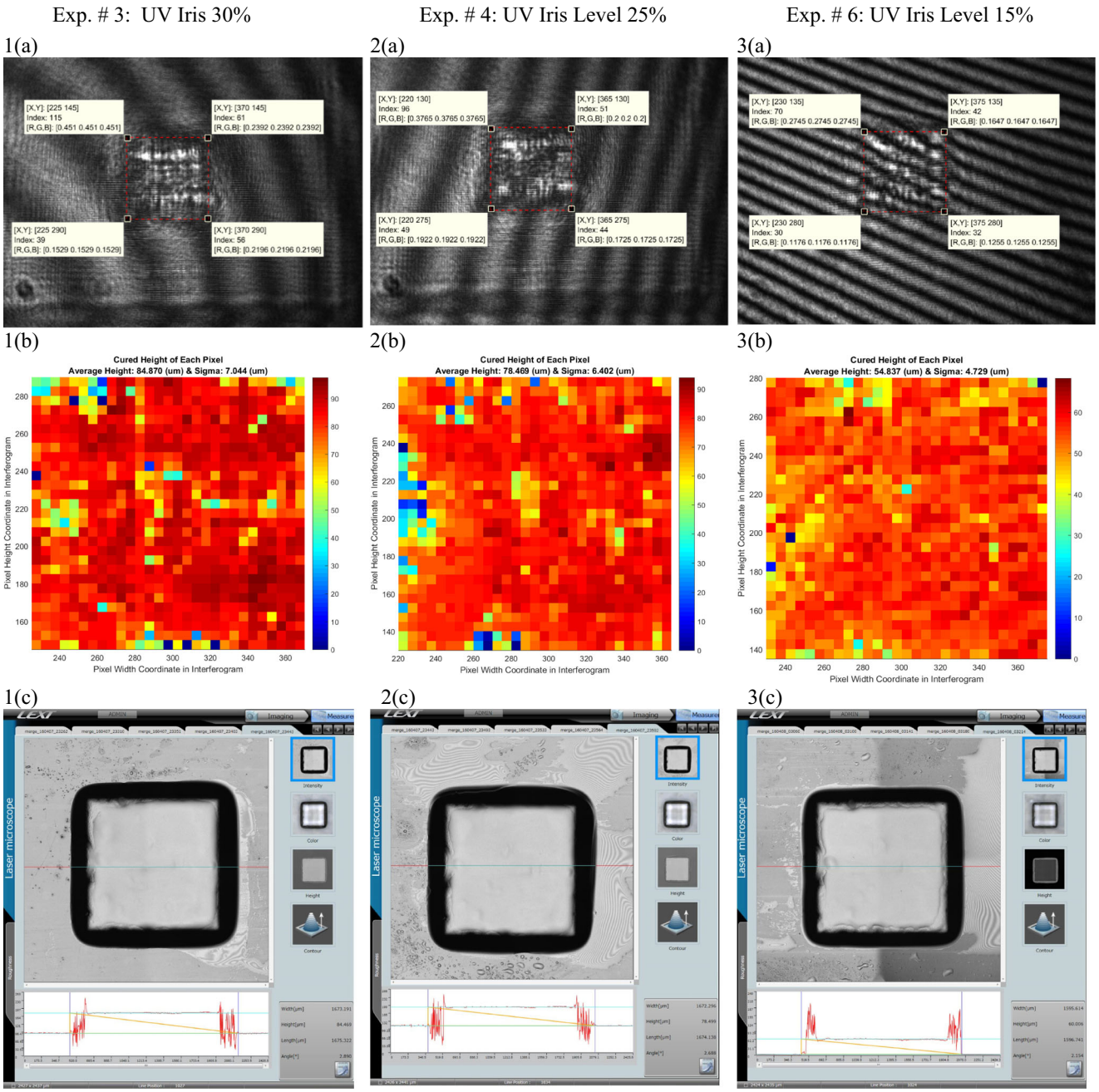

Fig. 10 Selected ICM&M result vs. microscope measurement for the *first set* of samples in exposure intensity experiment: *a* selected in the last interferogram the approximated cured area (*enclosed within the red dashed lines*) to measure with ICM&M; *b* ICM&M measured height profiles for voxels on the pixels within the cured area; *c* microscope-measured horizontal line profile. Exp. # 3 UV iris 30%. Exp. #4 UV iris level 25%. Exp. #6 UV iris level 15%

high (40%) intensity and lower intensity (5, 10, and 15%) had a larger relative error virtually within 10%.

The comparisons in Table 4 demonstrate the within-subgroup samples repeatability, between-subgroup trends of heights vs. intensity levels, and ICM&M estimation accuracy against microscope measurements. In each subgroup of experiments, the ICM&M results are close within the two samples and the microscope results are similar, but there seems to be a persistent gap between the ICM&M and microscope results. The alarming relative errors might be an indication for the need of using modified refractive index rather than constant refractive index in the ICM&M sensor model, which will be investigated in more details in an upcoming discussion about traceability in "Section 5.1."

The worst group which had the highest relative error is Experiment #7 at iris level 10%, but the absolute deviation is only about 4 μm that could be partially attributed

Table 4 Measurement results of validation experiments varying exposure intensity

Experiment subgroup no.	Exposure intensity (iris level) (%)	Sample no.	ROI cured area Pixels (width, height)	ICM&M results			Microscope measured profile line height (μm)			Absolute deviation (μm)	Relative error (%)
				Total phase (cycle, i.e., 2π rad)	Cured height (μm)	St. deviation—cured height σ(μm)	X-direction	Y-direction	Average		
Experiment #1	40	Sample 1	(220:365, 155:300)	8.453	*101.29*	4.86	95.939	94.620	**95.28**	6.01	6.30
		Sample 2	(220:365, 170:315)	8.562	*102.59*	7.26	97.043	96.964	**97.00**	5.59	5.76
Experiment #2	35	Sample 1	(225:370, 165:310)	7.639	*91.54*	6.48	92.001	93.153	**92.58**	−1.04	−1.13
		Sample 2	(220:365, 160:305)	7.500	*89.87*	7.20	88.997	90.060	**89.53**	0.34	0.38
Experiment #3	30	Sample 1	(225:370, 145:290)	7.083	*84.87*	7.04	84.469	82.695	**83.58**	1.29	1.54
		Sample 2	(225:370, 150:295)	7.122	*85.34*	6.54	83.884	84.793	**84.34**	1.00	1.18
Experiment #4	25	Sample 1	(220:365, 130:275)	6.549	*78.47*	6.40	78.499	77.905	**78.20**	0.27	0.34
		Sample 2	(225:370, 135:280)	6.611	*79.22*	5.91	77.958	77.368	**77.66**	1.55	2.00
Experiment #5	20	Sample 1	(235:380, 130:275)	5.665	*67.87*	5.59	69.762	70.258	**70.01**	−2.14	−3.05
		Sample 2	(235:380, 135:380)	5.502	*65.92*	5.74	70.277	66.826	**68.55**	−2.63	−3.84
Experiment #6	15	Sample 1	(230:375, 135:280)	4.577	*54.84*	4.73	60.006	58.985	**59.50**	−4.66	−7.83
		Sample 2	(230:375, 135:280)	4.923	*58.98*	4.83	62.812	64.431	**63.62**	−4.64	−7.29
Experiment #7	10	Sample 1	(230:375, 135:280)	3.409	*40.84*	4.50	45.653	45.658	**45.66**	−4.81	−10.54
		Sample 2	(225:370, 135:280)	3.456	*41.42*	4.47	45.646	45.342	**45.49**	−4.08	−8.96
Experiment #8	5	Sample 1	(225:370, 140:285)	2.307	*27.64*	5.40	30.895	28.620	**29.76**	−2.12	−7.12
		Sample 2	(235:380, 140:285)	2.312	*27.70*	5.20	30.019	28.666	**29.34**	−1.64	−5.61

to the microscope error. It is not unusual for the microscope cursor measurement to have a ±3μm or sometimes even up to 7-μm deviation from the average analysis of the microscope-exported spreadsheet of data. The smoother sample we have, the less error the microscope cursor measurement would have. The microscope error is more notable in the case of curing lower samples such as in Experiment #8 with iris level of 5%, only a 2-μm deviation would induce 7% relative error.

5 Measurement characteristics of ICM&M

5.1 Traceability

Metrological traceability is the property of a measurement result whereby the result can be related to a reference through a documented unbroken chain of calibrations, each contributing to the measurement uncertainty [17].

In the ICM&M practice, traceability is attained by careful calibration of the measurement system using the ICM&M sensor model to estimate the effective solid part refractive index as the calibrated transfer basis and using the microscope as a standard. With the experiment results above, the ICM&M traceability is reviewed and revised in this section to improve the overall measurement accuracy.

5.1.1 Best traceability achieved for same-condition samples

In the first set of validation experiments presented in "Section 4.3," the 12-s experiment had the best result with minimal errors (0.1 μm and less than 0.15%) in the full-field cured height profile, in which the outcome is within the expectation because it adopted exactly the same process conditions as the calibration did. The experiment concludes that the

ICM&M method could measure accurately for the ECPL process that is conducted with the same process conditions as the calibration experiment used.

5.1.2 Maintain traceability for different-conditions samples

Except for the 12-s exposure experiment in the first validation experiment group, all the other experiments were conducted with settings different from these in the calibration experiments. It is notable that the ICM&M estimation errors in these different-conditions samples display an interesting pattern—near-zero deviation for samples cured around the calibration experiment setting, smaller-than-actual (microscope) measurement result for samples cured with less time or less intensity, and larger-than-actual result for samples cured with more time or more intensity.

Specifically, in the first set of experiments varying exposure times (Table 3), the 9-s exposure experiment had a negative absolute deviation while the 15-s exposure experiments had positive values of absolute deviation. In the second set of experiments varying exposure intensity (Table 4) on the one hand, the ICM&M tends to overestimate the cured height in experiments with iris level from 40 to 25%, which are all larger than the 22% iris level intensity as was used in the calibration. On the other hand, the ICM&M tends to underestimate the cured heights in the less than 22% (i.e., 20, 15, 10, and 5%) experiments.

The observed pattern of deviations could imply that the effective refractive index for higher cured parts should be larger and that for lower cured parts should be smaller than the calibrated value of 1.4945 in the calibration experiments above, so that the ICM&M results could be brought closer to the microscope results.

Upon reflection on the definition of the mean (i.e., effective) refractive index n_m in the sensor model [10], we found that it was the intermediate value between the fully cured solid part's refractive index and the thin curing front's refractive index based on the mean value theorem of integration. Intuitively, the effective (i.e., mean) refractive index of the higher cured part could be larger as the cured part constitutes of more solid parts—the previously cured part with a larger curing degree and denser cross-linked polymers. As the part grows, the fresh cured thin layer occupies a less and less portion to the entire cured height; hence, the mean refractive index defined in the sensor model is expected to become larger.

The mean refractive index n_m is actually correlated with the cured height; hence, theoretically, it is subject to change during the curing process. The higher the cured part is, the larger the mean refractive index n_m. However, in the previous analysis as preliminary validation, for simplicity, we assumed that the mean refractive index was constant and modeled a linear relationship between the cured height and phase angle. The linear relationship due to the assumption of a constant refractive index sometimes does not hold well as one can see some nonlinearity present in the curing process from the dynamics curves in Figs. 7 and 9.

Reported investigations using the low coherence interferometry technique have confirmed the change in optical characteristics through the bulk of curing photopolymers [14, 18, 19].

For this specific ECPL material and process, to investigate quantitatively how the effective refractive index could be slightly changing as the photopolymerization curing goes on, we calculate the mean solid refractive index using the calibration model for all the samples and plot out the true effective refractive index against the ICM&M estimated phase angle as shown in Fig. 11. The model of effective refractive index of the in-process curing part and solid cured part is shown in Eq. (1) and Fig. 11. Both the trend and magnitude order (0.001) of the refractive index change found by the ICM&M analysis for the ECPL process conforms well with the literature-reported finding of a gradual increase in refractive index as the photopolymer resin cures [18], though different materials are used.

The reason we built the refractive index evolution curve against the phase angle instead of the cured height is because one would not have the height information available while implementing the ICM&M for height measurement, whereas the temporal phase shifts conveyed by the interferogram signals are accessible to provide an alternative indication for cured part growth.

There are a few outliers, for example, the data point of phase angle 4.75 with a refractive index of 1.4928 is from the exposure intensity experiment with UV iris level at 15%, for which refractive index estimation, we used the average of the two samples because it showed unusual

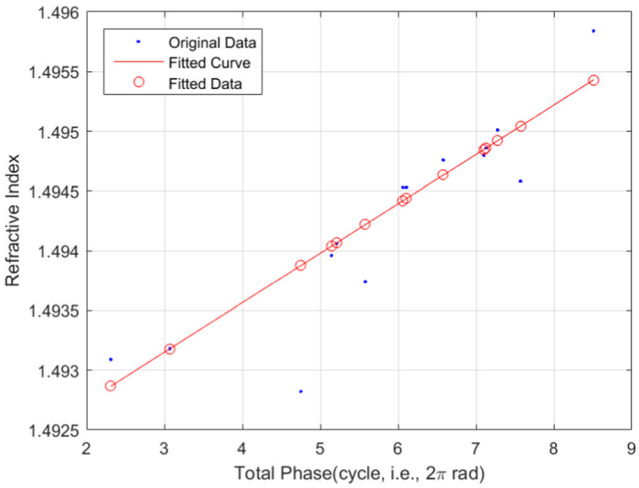

Fig. 11 Model of the evolving effective refractive index n_m

discrepancy. The main reason for the outliers lies in the microscope measurement uncertainty to which the subtle changing calibrated refractive index is very sensitive. Nevertheless, the *R*-square of the linear curve fitting is 0.95866, indicating a fairly good fitting. The coefficients in Eq. (1) show that the effective refractive index varies at the third decimal place, hence in the ICM&M method one should use a refractive index value accurate to at least the fourth digit after the decimal point.

$$n_m = 0.00041 \cdot \varnothing + 1.49191 \quad (1)$$

where n_m is the mean or effective refractive index of the cured part, and $\varnothing$ is the total shifted phase angle.

The overall ICM&M accuracy improvement with the evolving effective refractive index is shown in Fig. 12. The previously most-errored (10% error) group of 10% UV iris level experiment is now able to measure with under 5% error. After applying the improved model, the highest ICM&M errors presented in the 15% UV iris level experiment instead, which is understandable because its microscope measurements are the most inconsistent probably due to human error in the microscope practice.

5.2 Comparability and accuracy

External comparisons between the in-house ICM&M and a commercial microscope are an essential way to ensure commensurate measurements for evaluating the reliability of the developed ICM&M method. The experiments compare the ICM&M estimated height with the average of the microscope-measured profile line heights, resulting in absolute deviations and relative errors. The absolute errors of only a few microns and the relative errors under 5% prove that the ICM&M method has sufficient accuracy with a standard uncertainty of several microns for ECPL process measurement.

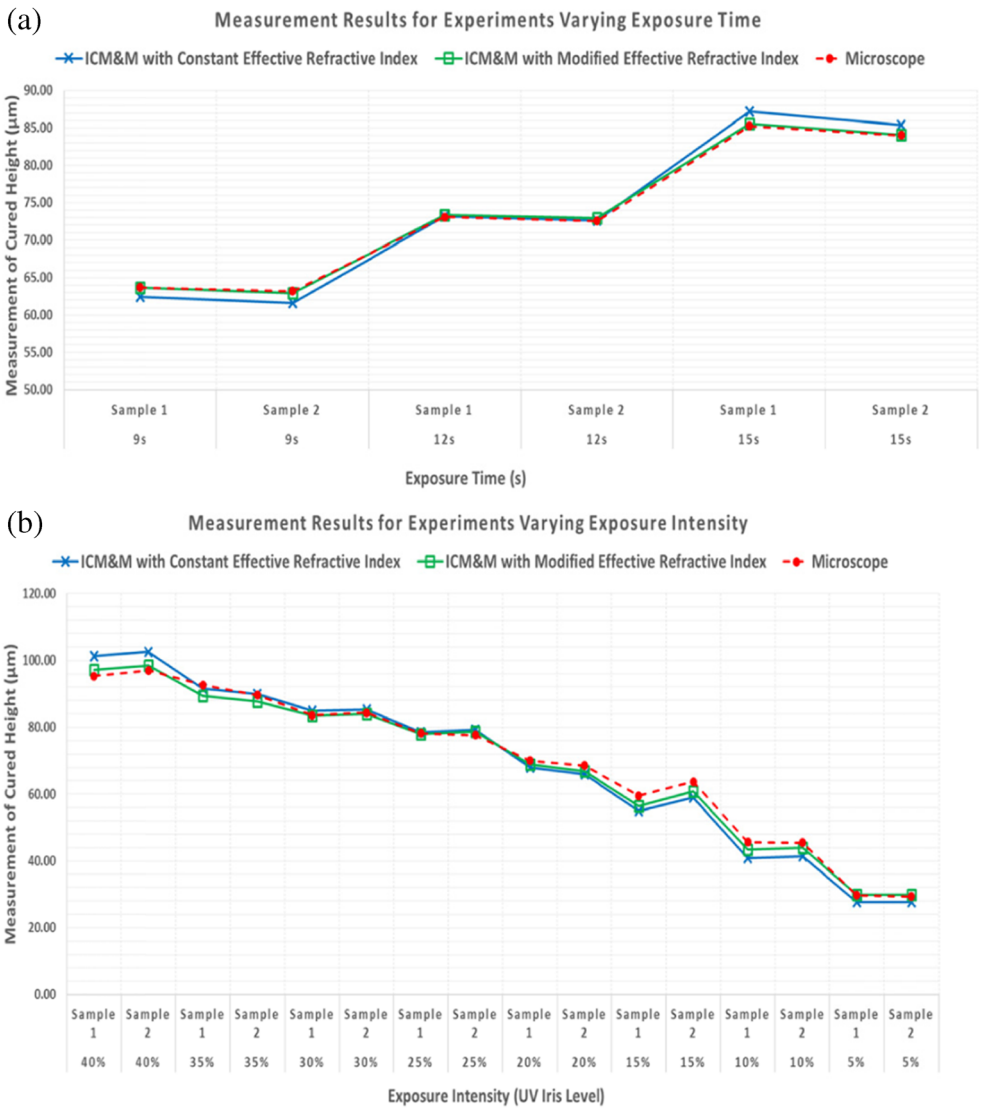

Fig. 12 Improved ICM&M accuracy by using growth-dependent (previously constant) effective refractive index in the sensor model (**a**) validation experiments varying exposure time; (**b**) validation experiments varying exposure intensity

The external comparison of ICM&M and microscope for each sample shows convincing accuracy of the ICM&M method.

Internal comparison results among the ICM&M measurements for various sample heights are also critical in the ICM&M validation to gain more confidence in its measurement capability. The samples in the calibration and validation experiments present consistency in the ECPL process output and ICM&M measurement results, which are shown to be good enough compared with the confocal microscope measurements.

All of the experiments including the ECPL process, ICM&M implementation, and microscope measurement, taken together, have established reproducible results and show comparability and consistency over space and time.

5.3 Repeatability

As shown in Tables 3 and 4 , the internal comparison of Sample 1 and Sample 2 in each subset of experiment shows quite identical ICM&M results of both phase angles and cured heights, which demonstrates the repeatability of the ICM&M method. In this study, the repeatability is computed as the square root of mean squared errors of the two samples in each experiment as shown in Eq. (2). Table 5 shows the repeatability of the two groups of validation experiments, and we could conclude that the ICM&M measurement repeatability is 2 μm, which means that one could expect a deviation of 2 μm in measurements for repeatedly cured samples' heights.

$$\text{Repeatability} = \sqrt[2]{\frac{\sum_{i=1}^{n}(Z_{i1}-Z_{i2})^2}{n}} \tag{2}$$

where n is the total number of experiment subsets, Z_{i1} and Z_{i2} are Sample 1 and Sample 2 heights, respectively.

5.4 Sensitivity, resolution, and range

Based on the ICM&M sensor model [10], the sensitivity of the measured height Z to the estimated phase change Φ is shown in Eq. (3) and evaluated as below. It indicates that an error of ±0.5 cycle in the phase estimation could induce an absolute deviation of ±6 μm in the height measurement. Due to the signal noise, the ICM&M algorithm sometimes could not identify the half cycle correctly, hence it happens that there could be a half-cycle variation in the phase estimation which explains partial reason for the observed variations of about 5 μm as shown in the ICM&M measurement results above (Figs. 8 and 10).

$$\frac{dZ}{d\varnothing} = \frac{\lambda}{2(n_m - n_l)} \cong \frac{0.532\mu m}{2(0.0222)} = 11.982\mu m \tag{3}$$

The ICM&M resolution is dependent on both the ECPL process speed and the ICM&M measurement speed, and the smallest cured height ICM&M could be estimated by Eq. (4).

$$\text{Resolution} = \frac{dZ}{d\varnothing}\cdot(\text{MTI}\cdot\text{IF}) \cong 11.982\cdot(\text{MTI}\cdot\text{IF})\,\mu m \tag{4}$$

where MTI is measurement time interval (s), and IF is the instantaneous frequency (Hz).

In this study, the measurement time interval is about 1/3 s and the ICM&M estimated instantaneous frequency vary with the exposure time and intensity. As is shown in Figs. 7 and 9, IF decreases as the curing goes on and as the intensity drops. In this study, the fastest curing occurs at the beginning of UV iris level 40% curing resulting in IF 1.4 Hz and the resolution is $11.982\cdot\left(\frac{1}{3}\cdot 1.4\right) = 5.59$ μm. The curing rate will slow down to zero at the end of the curing process with the resolution being gradually reduced to a couple of microns to ultimately less than 1 μm. For a mild exposure intensity such as 20–25% UV iris level, the curing process has the instantaneous frequency averaging at 0.5 Hz corresponding to a resolution of $11.982\cdot\left(\frac{1}{3}\cdot 0.5\right) = 2.00$ μm.

Generally speaking, the ICM&M method could discern vertical dimension measurement at a magnitude order of micron and has the ability to dive into submicron discrimination given a faster measurement speed.

The range characteristic of the ICM&M method is determined by the laser coherent length and the ECPL material property especially refractive index. In this study, it is obvious that the ICM&M method could measure part heights of up to at least 100 μm.

Table 5. Measurement repeatability

Validation Experiment Group	Repeatability (μm)	
	ICM&M	Microscope
#1 varying exposure time	1.16	0.82
#2 varying exposure intensity	1.82	2.01

6 Utility of the ICM&M system

6.1 Local vs. global measurement for the ECPL process

In Table 3, the line height, the area height average, and the microscope results are in good accordance for each sample, demonstrating two things: (1) a line could be representative to measure the average height of the entire cured area's average height; (2) the ICM&M is capable of both local and full-field

measurement for the average height of the cured part. However, the line profile results are shown to be sometimes worse than the area profile results in terms of accuracy, indicating the potential bias in sampling lines for estimating the average height of the cured part and the potential peril in controlling the cured part height with only a handful pixels' measurement average.

6.2 Lateral measurement potentiality

Though we focused on measuring the cured height in this study, a byproduct of lateral dimension measurement is also available. In all the experiments above, the resultant interferograms show a similar size of cured shape, which have approximately 145 pixels in the line corresponding to the flat top part's width in the microscope. Please note that the black outer frames around the samples as shown in Figs. 8 and 10 are sloping edges and are not taken into account for the width measurement by ICM&M, but might have been included in the microscope profile line. It is found that the width of the flat top part in all the samples is pretty close to 1250 μm, which could be directly seen in Fig. 8 Exp. #1 and Exp. #2.

All the experiments used the same size bitmap as DMD pattern (250 × 250 pixels), and the ICM&M method could retain that information of size similarity. Other than being able to qualitatively measure the lateral shape, the ICM&M is found to be able to measure quantitatively lateral dimensions according to the following calculations, which successfully estimated the width of the cured squares.

In an interferogram, one pixel is actually a binning of four original pixels captured by the ICM&M camera. The camera pixel size is 2.2 × 2.2 μm, hence a pixel in the interferogram is 8.8 × 8.8 μm. Because the ICM&M optics adopts a vertical beam path reflected upward from the sample to the camera, in principal, it is 1:1 mapping. The ICM&M measured lateral size could be estimated by multiplying the value of 8.8 μm with the number of pixels in the width dimension of the cured part shown in the interferogram. Hence, the estimated width of the cured square part is calculated as $145 \times 8.8 = 1276$ μm, which is in good accordance with the microscope measurement results of width: 1247.5 μm on average for the width of the flat top part in all the samples. The ICM&M width estimation result has 2.4% relative error with a deviation of 30 μm, which corresponds to ±4 interferogram pixels, which is acceptable for an initial study.

6.3 ICM&M for ECPL process dynamics, modeling, and control

Foremost, the two sets of experiment varying exposure time and intensity aim to verify the sensitivity of ICM&M method to the process input. The series of ICM&M detected grayscale signal and ICM&M estimated evolution of the instantaneous frequency and cured height in Figs. 7 and 9 exemplified that the ICM&M method could rapidly and accurately identify different ECPL process stages—threshold period, curing period, and dark period, and meanwhile could capture in a real-time fashion the process dynamics in terms of the curing speed (instantaneous frequency) and cured height. Hence, the ICM&M can provide a powerful tool for visualizing the process dynamics and help develop an insightful process model and thereby an effective process control system in the future.

In the validation experiments varying exposure times, the finding that the processes under all the same conditions but different exposure times share similar instantaneous frequency in the grayscale signal confirms that exposure time adjustment cannot manipulate the process dynamics such as curing rate. Hence, the conventional exposure time control of stereolithography-like additive manufacturing process is, strictly speaking, not a process dynamics control, but just a simple process on-off switch.

In the validation experiments varying exposure intensities, the evidence of the relationship between UV intensity and photo-curing process dynamics can be utilized for photopolymerization-based additive manufacturing process modeling and control. The new thinking of exposure intensity control could be a groundbreaking complement to the traditional exposure time control, in order to realize an ultimate control of the ECPL process for better accuracy.

7 Conclusion

The lack of real-time sensors critical to process monitoring and control has been identified as one of the major challenges that are currently impeding large-scale deployment of AM processes and equipment. The interferometric curing monitoring and measuring method, for the specific photopolymer-based micro stereolithography machine is validated and characterized in this study.

In this paper, to validate and fulfill the developed ICM&M method, an application program was designed and created in MATLAB. The application was deployed onto the physical system integrating the ECPL and ICM&M to automate the ECPL process. In this study, given the limited equipment configurations and computation resource, the data analysis and measurement computation in ICM&M was performed off-line. A coherent series of experiments were performed curing square samples by varying the factors of exposure time and intensity, and a representative full-field height profile was measured for each cured sample by both the in-house ICM&M and a commercial confocal microscope, to evaluate the measurement characteristics including traceability, comparability, accuracy, repeatability, sensitivity, resolution, and range.

The experimental results demonstrate that the ICM&M method can measure multiple voxel heights consistently and simultaneously and features the capability of full-field measurement which is desired in global measurement and control of ECPL. The ICM&M provides a cost-effective metrology for cured heights with excellent accuracy and repeatability and meanwhile features decent capability of estimating lateral dimensions. This off-line ICM&M experimental report is a convincing demonstration and advocacy for real-time ICM&M and can be used to benchmark the real-time ICM&M metrology. Once provided with a real-time operating system and multithread parallel computation power, the real-time process measurement and control for ECPL can be achieved with the aid of ICM&M method.

The experiment results also suggested for the development of an enhanced ICM&M sensor model with growth-dependent effective refractive index to improve its measurement accuracy.

In addition, utility of the ICM&M in process dynamics modeling and control was discussed. The ICM&M method successfully illustrated the ECPL curing process dynamics in terms of instantaneous frequency which is associated with the curing velocity, i.e., growing rate in units of micrometers per second. It is responsive to the curing start/stop, curing speed, and curing area as shown in the designed experiment series varying exposure time, intensity, and pattern size. The implementation with the well-developed MATLAB application demonstrates that the ICM&M is feasible and deployable in the physical system and fits well for the purpose for real-time ECPL process measurement, modeling, and control. Additionally, the ICM&M system is efficient compared with potentially available commercial measurement tools, which could be costly and needs retrofit to become a qualified real-time metrology for monitoring online photopolymer AM processes.

Acknowledgements This material is based upon the work supported by the National Science Foundation under Grant No. CMMI-1234561. Any opinions, findings, and conclusions or recommendations expressed in this publication are those of the authors and do not necessarily reflect the views of the National Science Foundation. All the related research is patent pending. The authors would also like to thank Jenny Wang, Changxuan Zhao, Will Borzon, Harrison Jones, and Dr. Amit Jariwala for their help with the experiment.

References

1. Measurement Science Roadmap for Metal-Based Additive Manufacturing (2013) National Institute of Standards and Technology (NIST)
2. Farshidianfar M, Khajepour A, Gerlich A (2016) Real-time control of microstructure in laser additive manufacturing. Int J Adv Manuf Technol 82(5–8):1173–1186. doi:10.1007/s00170-015-7423-5
3. Bikas H, Stavropoulos P, Chryssolouris G (2015) Additive manufacturing methods and modelling approaches: a critical review. Int J Adv Manuf Technol 83(1–4):389–405. doi:10.1007/s00170-015-7576-2
4. Jariwala AS (2013) Modeling and process planning for exposure controlled projection lithography. Ph.D. Dissertation, Georgia Institute of Technology, Atlanta, USA
5. Zhao X, Rosen DW (2016) Simulation study on evolutionary cycle to cycle time control of exposure controlled projection lithography. Rapid Prototyp J 22(3):456–464
6. Jones HH, Jariwala AS, Rosen DW (2014) Towards real time control of exposure controlled projection lithography. Proceedings of International Symposium on Flexible Automation
7. Jones HH, Kwatra A, Jariwala AS, Rosen DW (2013) Real-time selective monitoring of exposure controlled projection lithography. Proceedings of the 24th Solid Freeform Fabrication Symposium: 55–65
8. Jariwala AS, Schwerzel RE, Rosen DW (2011) Real-time interferometric monitoring system for exposure controlled projection lithography. Proceedings of the 22nd Solid Freeform Fabrication Symposium:99–108
9. Zhao X, Rosen DW (2015) Parameter estimation based real-time metrology for exposure controlled projection lithography. Proceedings of the 26th Annual International Solid Freeform Fabrication Symposium:1294–1312
10. Zhao X, Rosen DW (2016) Real-time interferometric monitoring and measuring of photopolymerization based stereolithographic additive manufacturing process: sensor model and algorithm. Meas Sci Technol 28(1). doi:10.1088/0957-0233/28/1/015001
11. The LEXT OLS4000 3D laser measuring microscope. http://www.olympus-ims.com/en/metrology/ols4000/. Accessed 09–10-2016
12. Colonna de Lega X (1997) Processing of non-stationary interference patterns—adapted phase-shifting algorithms and wavelet analysis. Application to dynamic deformation measurements by holographic and speckle interferometry. Swiss Federal Institute of Technology, Zürich, Switzerland
13. Tang Y (2005) Stereolithography cure process modeling. Georgia Institute of Technology, Atlanta
14. Arimoto H, Watanabe W, Masaki K, Fukuda T (2012) Measurement of refractive index change induced by dark reaction of photopolymer with digital holographic quantitative phase microscopy. Opt Commun 285(24):4911–4917
15. Lee JH, Prud'homme RK, Aksay IA (2001) Cure depth in photopolymerization: experiments and theory. J Mater Res 16(21):3536–3544
16. Jacobs PF (1992) Rapid prototyping and manufacturing: fundamentals of stereoLithography. Society of Manufacturing Engineers, Michigan, United States
17. Korpelainen V (2014) Traceability for nanometre scale measurements—atomic force microscopes in dimensional nanometrology. University of Helsinki, Finland
18. Hadis MA, Tomlins PH, Shortall AC, Palin WM (2010) Dynamic monitoring of refractive index change through photoactive resins. Dent Mater 26(11):1106–1112
19. Tomlins PH, Palin WM, Shortall AC, Wang RK (2007) Time-resolved simultaneous measurement of group index and physical thickness during photopolymerization of resin-based dental composite. J Biomed Opt 12(1):014020